ACS APPLIED NANO MATERIALS

www.acsanm.org Article

Hydrocarbon Diffusion in Mesoporous Carbon Materials: Implications for Unconventional Gas Recovery

Yann Magnin,* Jérémie Berthonneau, Nicolas Chanut, Daniel Ferry, Olivier Grauby, Rachel Jorand, Franz Joseph Ulm, Eric Chaput, and Roland Pellenq

Cite This: *ACS Appl. Nano Mater.* 2020, 3, 7604−7610 Read Online

ACCESS | Metrics & More | Article Recommendations

ABSTRACT: Methane diffusion in micro- and mesopores of carbonaceous materials is dominated by molecular interactions with the pore walls. As a consequence, the fluid molecules are mainly in a diffusive regime and the laws of fluid mechanics are not directly applicable. A method called the "free volume theory" has been successfully used by different authors to study the diffusion of *n*-alkanes into microporous carbons. However, we show in this paper that such a method fails to describe the dynamical properties of methane in porous hosts presenting both micro- and mesopores. We further evidence that this theory is limited to structures whose pore diameters are lower than ∼3 nm. We then propose a simple scaling method based on the micro- and mesoporous volume fraction in order to predict diffusion coefficients. This method only requires the knowledge of (i) the host microporous volume fraction and (ii) the self-diffusion coefficient in micropores smaller than 3 nm, which can be obtained using the "free volume theory", quasi-elastic neutron scattering experiments, or atomistic simulations.

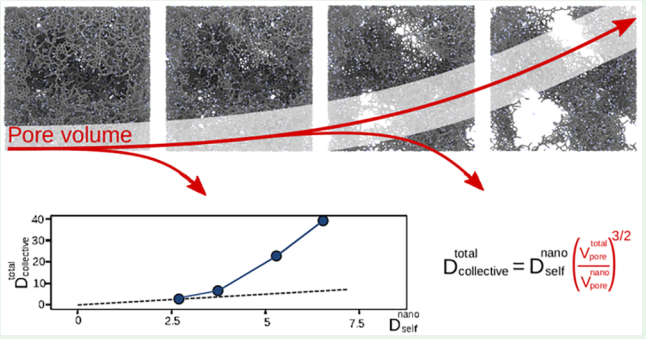

KEYWORDS: *Molecular diffusion, Kerogen, Methane, Green−Kubo equation, Molecular dynamics, Tomography*

INTRODUCTION

Unconventional hydrocarbon recovery has attracted much attention during the last decades. In the United States, it has reached around 69% of the natural gas produced in 2018, compared to 1% in 2000.[1,2] However, an exponential production decline is observed on some reservoirs during the exploitation process, which is not captured by conventional reservoir modeling tools.[3,4] This behavior is not fully understood due to a general lack of knowledge about hydrocarbon behavior in the deep underground, and typically, a reservoir can be exploited for a few years before being fracked again in order to be revitalized. In such reservoirs, hydrocarbon molecules are trapped into unconnected pockets of porous organic matter called kerogen.[5,6] These pockets, typically a few dozen μm, are dispersed into a mineral matrix located in deep underground shale formations. Hydrocarbon molecules are trapped in the microporosity (≤2 nm), mesoporosity (in between 2 and 50 nm), and macroporosity (>50 nm) (along the line of the IUPAC classification)[7] of the heterogeneous porous network of kerogens, presenting complex tortuosity, connectivity, and constrictivity.[8,9]

The transport of fluids in macroporous media is well described by Darcy's law,

$$\mathbf{v} = -\underbrace{\frac{k}{\eta}}_{K}\nabla P \tag{1}$$

which is derived from the Navier−Stokes equation. In eq 1, the flow velocity $\mathbf{v}$ scales linearly with the pressure gradient ∇P, and depends on the permeability of the porous network k, and the molecular viscosity η. However, for pores below 50 nm, Darcy's law fails to describe the fluid transport, which is mainly governed by adsorbate/adsorbent interactions.[10−12] For the same reason, macroscopic fluid mechanics techniques such as Lattice Boltzmann Method (LBM) and Computational Fluid Dynamics (CFD) (essentially consisting of solving the Navier−Stokes equation) also fall short in describing the diffusion properties in pore diameters below 50 nm. At this scale, these techniques have to be modified in order to incorporate properties such as slippage, friction, surface tension, adsorption, and nonviscous effects that dominate

Received: May 6, 2020
Accepted: July 6, 2020
Published: July 6, 2020

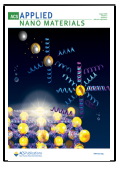

https://dx.doi.org/10.1021/acsanm.0c01191
ACS Appl. Nano Mater. 2020, 3, 7604−7610

and are generally neglected by the fluid mechanics.[10,13−15] For example, corrections like the Klinkenberg effect that accounts for slippage have been included in Darcy's equation.[16] However, such an empirical correction does not capture the phenomenon of molecule adsorption with the pore walls, paramount to describing the transport behavior. Thus, eq 1 and its corrected versions are unsuitable in micro- and mesoporous systems. In this pore size range, adsorption tends to increase the fluid density, and molecules therefore present different properties than in the bulk phase.[17] In micropores, the Free Volume Theory (FVT) was shown to be a robust theoretical model for predicting the diffusion of highly confined molecules.[10,13,18,19] Falk et al.[17] evidenced a linear dependence of $\mathbf{v}$ by replacing the permeability and the viscosity in eq 1 by a parameter called "permeance" defined as $K = D_s/(\rho k_B T)$, with D_s the self-diffusion coefficient of molecules, ρ the molecular density, and $k_B T$ the thermal energy of the system. From Equilibrium Molecular Dynamic (EMD) simulations, they showed that K collapses on a master curve for different n-alkane lengths, in a large pressure range.[10] EMD simulations were further compared to Non Equilibrium Molecular Dynamics (NEMD) simulations, with a good agreement.

In this article, we first determine the FVT limitation in synthetic pores of constant diameters H, filled by methane molecules. We show that for $H > 3$ nm, the FVT is no longer suitable. We then focus on microporous atomistic kerogen structures, in which experimentally observed mesopores up to 3 nm are introduced from electron tomography reconstruction. Such experimental pore size distribution has been chosen to stay below the upper limit of the FVT (pore diameters of about 3 nm). This pore size is then scaled in order to study the effect of increasing mesoporous volume in the structure, while maintaining the porous topology. Doing so, we highlight a deviation from the FVT due to weaker adsorption in mesopores. We then propose a scaling method able to approximate the self- and collective diffusion coefficients at the mesoscale from the ones at the microscale, by linking the diffusion coefficients to the microporous volume fraction. Such a correction is determined from a basic set of experimental or numerical data: the fluid loading and the kerogen pore size distribution. Thus, the FVT can be used to determine diffusion coefficients in the microporosity of the porous host,[10,19] which are then upscaled to account for the effect of mesopores.

RESULTS AND DISCUSSION

At the macroscale, where collective interactions between molecules dominate, the transport is convective and well described by fluid mechanics laws. At the microscale (pore diameter <2 nm), in a very confined environment, the transport is diffusive and the convective contribution is negligible.[20,21] In other words, confined molecules in micropores have only a very limited number of neighbors, and diffusion is thus mainly governed by the interactions between the molecular fluid and the pore walls.[10] In order to study methane diffusion into kerogens, we performed EMD simulations with unconstrained kerogen structures in the N,P,T ensemble, and determined the fluctuations of the total momentum via the Green−Kubo equation[22]

$$D_c = \underbrace{\frac{V}{Nk_BT}\sum_k \int_0^\infty \langle \mathbf{v}_k(t).\,\mathbf{v}_k(0)\rangle_{eq}\,dt}_{D_s} + \underbrace{\frac{V}{Nk_BT}\sum_{k\neq k'} \int_0^\infty \langle \mathbf{v}_k(t).\,\mathbf{v}_{k'}(0)\rangle_{eq}\,dt}_{\text{cross correlation}} \quad (2)$$

In eq 2, N is the number of methane molecules, V the volume of the system, and $v_k(t)$ the center of mass velocity of molecules k. D_s and D_c correspond to the self- and collective diffusion coefficients, respectively.

As can be seen in eq 2, when molecules are highly confined, with a very limited number of neighbors, cross correlations may be neglected and $D_c \sim D_s$. In such a case, the adsorption of a single molecule in a porous medium can be described as a slip friction force $f = -\xi^{(0)}v^{(0)}$, with $\xi^{(0)}$ and $v^{(0)}$ the friction coefficient and the velocity of the molecule, respectively. The self-diffusion of methane thus reads as

$$D_s = D_s^{(0)} \exp\left[-\alpha\frac{NV_{CH_4}}{V}\right] \quad \text{with } D_s^{(0)} = \frac{k_BT}{\xi^{(0)}} \quad (3)$$

where $D_s^{(0)}$ is the self-diffusion coefficient of a single molecule (here methane), α a coefficient accounting for molecular overlaps, N the number of molecules, V_{CH_4} the minimum void size volume allowing for a molecule to move into it (corresponding approximately to the molecular size), and V the accessible free volume into the porous host.

The FVT[23] provides an analytical expression describing the probability that molecules find a free cavity around them. In sufficiently small pores, when this probability (scaling as an exponential) is multiplied by the self-diffusion coefficient of a single molecule $D_s^{(0)}$, and the eq 3 allows for approximating the self-diffusion coefficient D_s of N adsorbed molecules.

Note that such an approach has been generalized for single fluid component and mixtures by Obliger et al.,[19] in order to be used with the sole knowledge of the host porosity, the molecular loading, and the molecular size.

Synthetic Structures. As described above, the FVT has been successfully used in microporous kerogens.[19] However, its validity has never been questioned in the presence of mesopores. For the sake of simplicity, we first use synthetic tortuous cylindrical pores with constant diameters (Figure 1A). Configurations were built by randomly moving a sphere of diameter H (ranging from 1 to 5 nm) into a dense kerogen structure (with a density $\rho \sim 1.4$ g/cm^3), where the microporosity is smaller than the methane kinetic diameter. The corresponding pore size distributions were determined by particle insertion corresponding to the kinetic diameter of methane, using the method proposed by Bhattacharya et al.[24] (Figure 1B). Methane molecules are then adsorbed into the cylindrical pores by the Grand Canonical Monte Carlo technique for two fluid loading corresponding to $\Gamma_{CH_4} = 0.25$ and 0.5. EMD is then performed to determine diffusion coefficients from eq 2. In Figure 1C, we show D_c as a function of D_s for different H. When $H < 3$ nm, $D_c \sim D_s$ for both loadings. Indeed, in this H range, molecules are highly confined, and cross correlations in eq 2 are negligible due to the lack of intermolecular interactions. In this case, the adsorption governs diffusion and the FVT can be applied. However, for $H > 3$ nm, we observe a deviation from the master curve. This behavior comes from finite cross correlations in eq 2, when H increases. In this case, fluid

https://dx.doi.org/10.1021/acsanm.0c01191
ACS Appl. Nano Mater. 2020, 3, 7604−7610

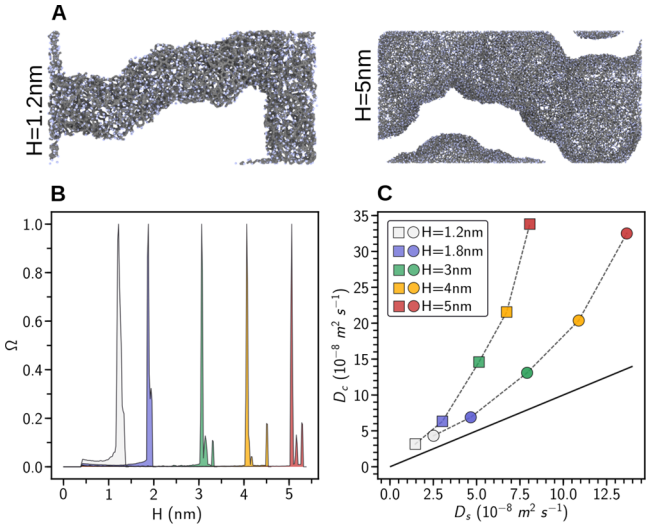

Figure 1. A. Snapshots of two pores shaped by moving a sphere of diameter H into a dense kerogen structure. B. Pore size distribution determined by methane molecules insertion for the different synthetic structures. C. Collective diffusion coefficients as a function of the self-diffusion coefficients for the different pore diameters. Two molecular loadings are compared, Γ_{CH_4} = 0.25 (circles) and Γ_{CH_4} = 0.5 (squares). Each plot is compared to the linear master curve (black line) highlighting the influence of the cross correlations in the Green–Kubo equation, and thus the validity of the FVT. Colored symbols correspond to pore diameters H = 1.2 nm (light gray), H = 1.8 nm (blue), H = 3 nm (green), H = 4 nm (yellow), H = 5 nm (red).

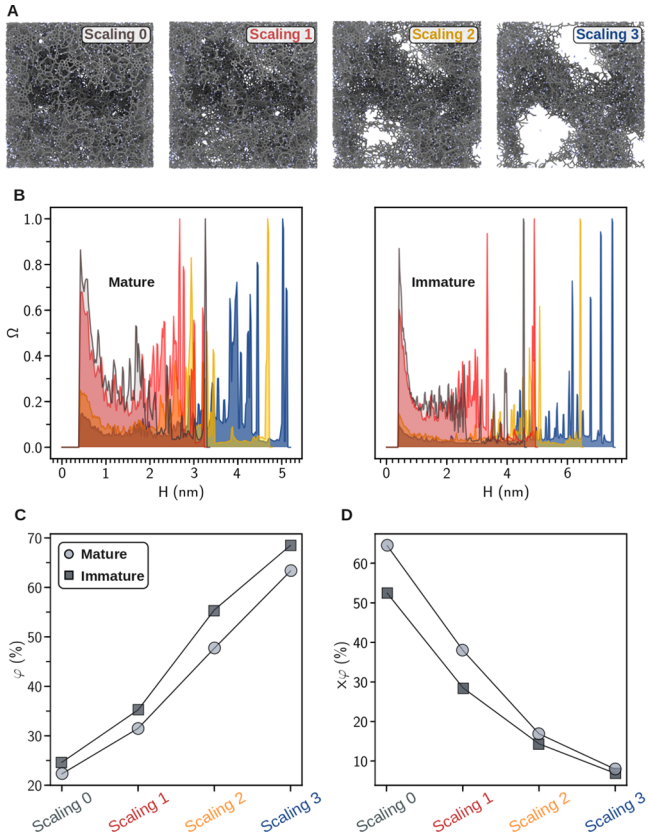

Figure 2. A. Snapshots of mature kerogen structures for the four scaling applied to increase the mesoporous volume. B. Pore size distribution determined by methane molecule insertion for the four generated structures in mature (left) and immature kerogens (right). Brown, red, yellow, and blue plots correspond to scalings 0 (original porosity measured by electron tomography), 1, 2, and 3, respectively. C. Evolution of the porous volume as a function of the scaling for matures (circles) and immature kerogens (squares). D. Evolution of the microporous volume fraction as a function of the scaling for matures (circles) and immature kerogens (squares).

molecules are less sensitive to adsorption and the FVT does not apply anymore. Note that for H < 3 nm, D_c as a function of D_s slightly deviates from the master curve. It was already noticed by Falk et al.,[10] and this behavior originates from a relatively low methane adsorption compared to longer *n*-alkanes, which merge on the master curve.

Kerogen Structures. The same calculations were then performed in atomistic kerogen structures, Figure 2A. These configurations were built by cropping 3D mesopores measured experimentally in kerogen structures. We used electron tomography to reconstruct the actual mesoporous network of a kerogen sample extracted from a productive gas-prone shale formation (further details on the sample, acquisition, and procedure are given in the Methods). Such a methodology based on experiments has been established in order to produce realistic atomistic structures accounting for the complex pore topology encountered in real kerogen samples such as tortuosity, connectivity, and constrictivity. In order to investigate the effect of the mesoporosity on the diffusion coefficients, we scaled the mesoporous volumes by removing a certain thickness from the surface of the pores. This allowed us to study the effect of the pore size and volume, while maintaining the topology of the structure. We thus built four kerogen structures referred as scaling 0 (original porosity measured by electron tomography) to scaling 3, corresponding to the largest mesoporous volume. Such methodology was applied for a mature and immature kerogen, corresponding to a rigid aromatic carbonaceous structure and an aliphatic flexible one, respectively.[25,26] The methodology developed to produce such atomistic structures is detailed in the section Methods.

As previously described, methane molecules are adsorbed by the Grand Canonical Monte Carlo technique for a molecular loading Γ_{CH_4} = 0.5. A full atom equilibration is then performed by EMD in the (N,P,T) ensemble in order to relax the filled structures. The volume of the mature kerogens were found to marginally increase through methane adsorption, while it induces a swelling of the immature ones.

The Figure 2B shows the pore size distributions[24] Ω for all generated structures, highlighting the presence of micro- and mesopores in all cases, with a maximum pore diameter of $H \sim$ 7 nm for scaling 3 of the immature kerogen. The porosity φ is shown in Figure 2C as a function of the scaling with φ ranging from ∼20% (scaling 0) to ∼70% (scaling 3). The microporous fraction x_φ corresponds to the ratio of micropores in a structure compared to the entire pore volume, defined as

$$x_\varphi = \frac{\int_0^{3\text{nm}} \Omega \, dH}{\int_0^{\infty} \Omega \, dH} \tag{4}$$

and varies reversely to φ, from ∼65% (scaling 0) to ∼8% (scaling 3). Indeed, increasing the mesoporous volume concomitantly leads to a decrease of the microporous volume fraction into the structures (Figure 2D).

In order to link the diffusion to the textural properties of the kerogens, we further study the evolution of the self- and

https://dx.doi.org/10.1021/acsanm.0c01191
ACS Appl. Nano Mater. 2020, 3, 7604−7610

collective diffusion coefficients with the microporous volume fractions. On one hand, we show that the ratio of the self-diffusion coefficients at the micro- and mesoscale, respectively, $D_s^{(n)}$ and D_s, scales as the square root of the microporous fraction x_φ (Figure 3A), such as

$$\frac{D_s^{(n)}}{D_s} \sim \sqrt{x_\varphi} \tag{5}$$

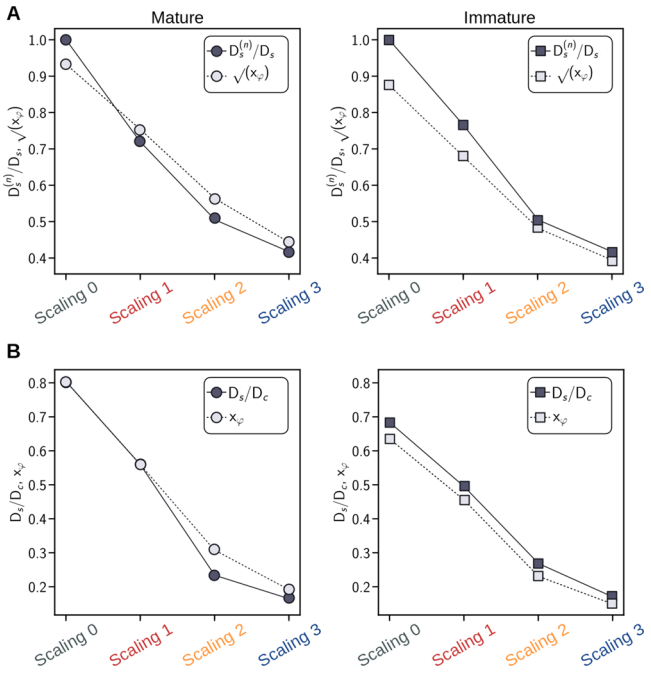

Figure 3. A. Ratio of the self-diffusion coefficient in a fully microporous structure and the self-diffusion coefficient in micro- and mesoporous structures $D_s^{(n)}/D_s$ as a function of the scaling for mature (dark gray circles) and immature kerogens (dark gray squares). The dashed line show the evolution of the square root of the microporous volume fraction for each scaling for the mature (light gray circles) and immature kerogens (light gray squares). B. Ratio of the self- and collective diffusion coefficients D_s/D_c as a function of the scaling for mature (dark gray circles) and immature kerogens (dark gray squares). The dashed line show the evolution of the microporous volume fraction for each scaling for the mature (light gray circles) and immature (light gray squares).

where $D_s^{(n)}$ can be obtained from the FVT, from EMD simulations or from Quasi-Elastic Neutron Scattering experiments, and further be used to determine D_s with the sole knowledge of x_φ. On the other hand, we show that the ratio of the self- and collective diffusion coefficients at the mesoscale, respectively, D_s and D_c, scales with the microporous volume fraction x_φ (Figure 3B), such as,

$$\frac{D_s}{D_c} \sim x_\varphi \tag{6}$$

By combining eq 5 and eq 6, D_c can thus be readily determined with

$$D_c = D_s^{(n)} x_\varphi^{-3/2} \tag{7}$$

This observation allows us to develop an upscaling method enabling the determination of the diffusion coefficients in materials containing both micro- and mesopores, with a minimal set of experimental or numerical data. In Figure 4A, we show the upscaling procedure for the case of mature

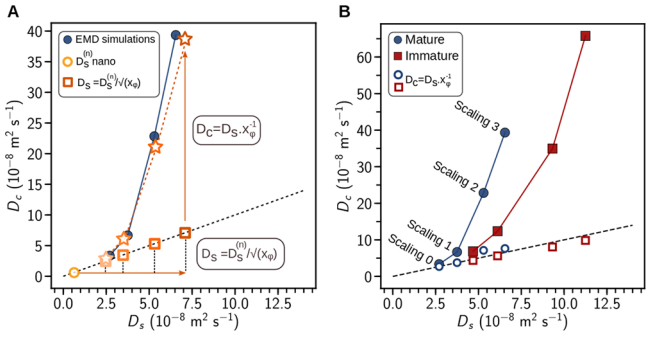

Figure 4. A. Collective diffusion coefficient D_c as a function of the self-diffusion coefficient D_s for the different scalings in mature kerogens. The empty yellow circle corresponds to a fully microporous kerogen structure (before the introduction of mesoporosity by electron tomography). Self-diffusion at microscale $D_s^{(n)}$ is first upscaled using eq 5 in order to get D_s for the different scalings (orange squares), reported on the master curve (dashed black line). D_s are then used to determine D_c with the eq 6 for the different scalings (orange stars). D_c determined by EMD simulations are presented for comparison (filled blue circles). B. D_c as a function of D_s determined by EMD simulations for different scalings in mature (filled blue circles) and immature (filled red squares) kerogens. The reverse scaling from the numerical simulations for mature (empty blue circles) and immature (empty red squares) is shown to merge on the master curve (dashed black line).

kerogens. First, the diffusion coefficients are determined into the fully microporous kerogen (yellow circle). The eq 5 is then used to determine D_s from $D_s^{(n)}$ for the different mesopore scaling using x_φ, which is calculated from the pore size distributions using eq 4. In the scaled structures, diffusion coefficients follow the same behavior than in the synthetic pores presented above, with a deviation from the master curve when the pore volume increases (x_φ decreases). Note, however, that the original kerogen structure (scaling 0) is located on the master curve despite the presence of a small mesoporosity (Figure 4A,B). This shows that the diffusion behavior is dominated by the presence of micropores when x_φ is larger than ~50% (Figure 2D). It suggests that the FVT could potentially be applied in structures containing an abundant fraction of micropores. For the structures that deviate from the master curve, once D_s is known (orange squares in Figure 4A), we use eq 6 to determine D_c. The deviation from the master curve thus corresponds to the cross correlation contribution in the eq 2, arising from the increasing mesoporous volume. Finally, we compare the results of the upscaling approach (empty orange stars) to the EMD simulations (filled blue circles) with a good agreement, highlighting the robustness of the method.

By further comparing the results in the mature and immature structures (Figure 4B), we see that D_s is larger in immature kerogens than in mature ones, with a more pronounced deviation from the master curve. This behavior is not surprising because flexible immature structures swell when adsorbing methane molecules into their porous networks, leading to larger diffusion coefficients.[27] In immature kerogen structures, the full upscaling procedure is not possible as these structures do not contain micropores larger than the kinetic diameter of methane. However, we show that D_c can be

https://dx.doi.org/10.1021/acsanm.0c01191
ACS Appl. Nano Mater. 2020, 3, 7604−7610

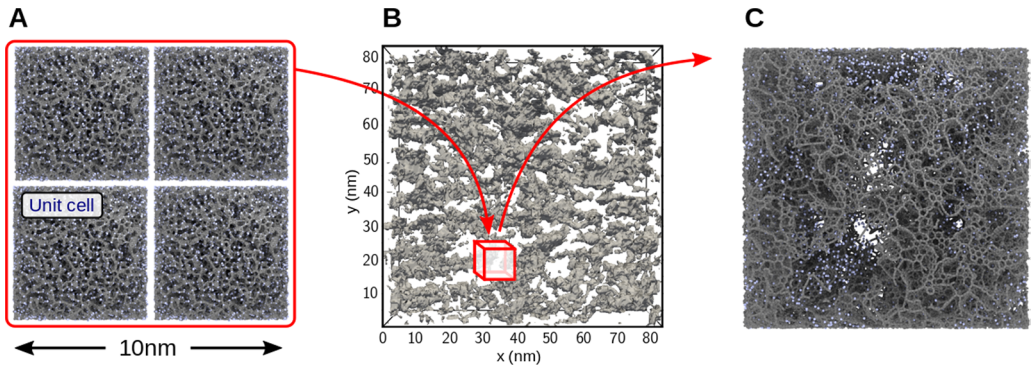

Figure 5. (A) Kerogen unit cell with 5 nm edges. (B) 3D distribution of mesopores as reconstructed by electron tomography. (C) Atomistic kerogen structure with 10 nm edges, embedding both micro- and mesopores from experiments.

determined from the master curve with eq 6, highlighting the consistency of this scaling procedure for both structures.

CONCLUSIONS

In this paper, we propose a simple method to scale diffusion coefficients of methane molecules into porous kerogen structures from the micro- to the mesoscale. At the microscale, diffusion is mainly governed by the adsorbate/adsorbent interactions, and the dynamical behavior of a molecular fluid is mainly diffusive. In this case, the free volume theory has been successfully used to determine the molecular diffusion coefficients. In this work, we first evaluated the ability of the free volume theory to predict the molecular diffusion of methane in synthetic mesoporous structures, highlighting its breakdown for pores above 3 nm. We then performed simulations in realistic mature and immature kerogen structures, where the mesoporosity (up to 3 nm) has been introduced by means of electron tomography. The resulting micro/mesoporous structures have then been scaled (up to 7 nm), allowing us to evidence an increase of diffusion coefficients with the pore volumes due to the emergence of the intermolecular collective interactions.

We then proposed a scaling methodology where the diffusion coefficients in mature and immature micro/mesoporous structures can be well-approximated with the sole knowledge of the self-diffusion coefficients at the microscale and the microporous volume fraction. Such a method can be used from experiments, simulations or directly from the free volume theory, with the advantage of using a minimal set of experimental or numerical data.

While we focused on hydrocarbon diffusion in kerogen structures, we think that such a method could be used in a variety of applications involving disordered porous systems with different chemistry. Potential candidates include electrical energy storage (EES) systems such as Li-ion batteries[28] and supercapacitors,[29] catalysts and adsorbents for separation processes,[30,31] or membranes in biological systems.

The materials used in the applications mentioned above are generally multiscale porous materials. In order to study diffusion into such materials, it is worth noting that hybrid molecular dynamics and Lattice Boltzmann Method (LBM) have been successfully used to predict diffusion coefficients.[32] This approach is however challenging due to expensive computational times necessary to determine the diffusion at the micro- and mesoscale by molecular dynamics, prior to their introduction in the LBM. We thus think that a simple method such as the upscaling technique developed in this work could be helpful in multiscale LBM simulations.

METHODS

The mesoporous kerogen structures are designed from a microporous unit-cell carbon structures with 5 nm edges (Figure 5A). We used two different structures referred as mature and immature kerogens. The mature one is mainly aromatic, with a Young's modulus ∼45 GPa, while the immature structure is aliphatic, with a Young's modulus ∼2 GPa. While the mature structure is rigid, the immature one is more flexible and will swell when filled with molecules. Thus, flexibility in immature kerogens has to be accounted for in order to be consistent with real samples. Swelling in mature kerogens is generally assumed to be limited and is usually neglected.

Unit-cell structures were generated by Obliger and Leyssal et al. from a liquid quench molecular dynamics technique described in detail elsewhere.[26] The basic idea to generate such structures is to start from a random distribution of carbon and hydrogen atoms on a cubic lattice. For the sake of simplicity, heteroatoms such as O, N, and S are neglected due to their small effects on poromechanical properties. Structures are then simulated at high temperature ($T \sim$ 6000 K), during a few ps in the canonical ensemble (N,V,T), where N is the number of atoms in a structure, V the volume of the system, and T the temperature. Once the structure is melted, a linear temperature damp is performed down to T = 300 K at a predefined quench rate. Resulting structures are thus porous carbonaceous materials that can be reasonably compared to microporous kerogen.[26]

Such kerogen unit-cells are then duplicated along the x, y, and z directions to form a $10 \times 10 \times 10$ nm^3 kerogen structure (Figure 5A). Mesopores are included from a 3D experimental reconstruction of the mesoporous network obtained from electron tomography (Figure 5B). As described in the work of Berthonneau et al.,[9] a thin section of kerogen sample is first extracted from the Marcellus shale formation (PA, USA) with a focused ion beam (FIB, FEI Helios NanoLab 660). The kerogen pore network is then imaged and reconstructed in 3D with a transmission electron microscope (TEM, Jeol JEM-2010) equipped with a LaB_6 electron gun, under a 200 kV accelerating voltage, and assisted by the Digital Micrograph software (GATAN Image suite ver. 2.31). A Tilt series of bright field 2D projections is recorded with a CCD camera (GATAN, Ultrascan 1000XP model 994), aligned with a cross correlation procedure implemented in the software, and reconstructed in the Fourier space by the Weighted-Back-Projection (WBP) method. A denoising procedure using "Non-Local Mean Denoising" and "Median" image processing filters is then performed, relying on the comparison between a reference image (i.e., the original image acquired at 0°) and the summation of the reconstruction according to the z direction. The filtering parameters are varied in order to optimize the peak signal-to-noise ratio between the reference image and the filtered one. Once the optimal filtering condition is found, a segmentation of the pore network is conducted by "Otsu thresholding" of the filtered reconstruction's gray level histogram. The resulting 3D reconstruction, or tomogram, comprises

https://dx.doi.org/10.1021/acsanm.0c01191
ACS Appl. Nano Mater. 2020, 3, 7604−7610

a stack of binary images with dimensions of 210 × 210 × 21 nm^3, containing the organic mesoporous network. After being cropped to the appropriate dimensions of the duplicated kerogen unit-cells (Figure 5A,B), the imaged network served as a mask to carve mesopores. Hence, imaged mesopores are added to the structural micropores of the kerogen unit-cells to produce the atomistic kerogen structures containing both micro- and mesopores (Figure 5C). This coupling thus provides a resolution overlap to the input models. As a consequence, if a fraction of the micropores were below the resolution limit of the TEM, they are rightfully modeled by the atomistic reconstruction of the kerogen unit-cell. The advantage of using such experimental data is to keep a realistic pore topology in order to study the dynamical behavior of fluid molecules into mesoporous structures as described above. In kerogen samples, the pore size usually ranges from the microscale to macroscale, with a large fraction of mesopores of a few nanometers.[8] In order to connect our simulations to the FVT approach, we first choose an area in the tomogram, where the mesoporosity is relatively small (~2−3 nm). Mesopores were then scaled up to study the effect of mesopore sizes on the dynamical properties of adsorbate molecules (Figure 2A).

The final structure shown in Figure 5C contains approximately 10^5 atoms. It is used to produce structures with larger mesoporous volumes, keeping a similar pore texture. Practically, for each structure produced (referred to as scaling 0, 1, 2 and 3), we scaled up the mesoporosity by removing atoms located at a distance δ from mesopore surfaces. Thus, each scaling shown in the Figure 2A corresponds to structures where δ is increased by 0.8 nm steps for each scaled pore.

Methane adsorption is performed by Monte Carlo simulations in the Grand Canonical ensemble (μ_{CH_4},V,T).[33] In this technique, the kerogen structure randomly exchanges molecules with an ideal gas reservoir at a constant methane chemical potential (μ_{CH_4}), volume (V), and temperature (T). The system is equilibrated during 10^6 cycles. A cycle consists of trying 1000 molecule insertions or deletions. Insertions or deletions are randomly selected at each cycle with 50% probability. Thus, the fluid density depends on the thermodynamic parameters (μ_{CH_4},V,T).

In simulations, C and H interact via the long-range bond order potential AIREBO,[34] while methane−kerogen and methane−methane interactions are modeled with a Lennard-Jones potential and the CH_4 molecules are considered as pseudoatoms.

$$U = 4\epsilon_{ij}\left[\left(\frac{\sigma}{r_{ij}}\right)^{12} - \left(\frac{\sigma}{r_{ij}}\right)^{6}\right] \tag{8}$$

In this potential, σ is the atomic kinetic diameter, r_{ij} the interatomic distance, and ϵ_{ij} is the interaction energy between two atoms i and j. The Lennard-Jones parameters (see Table 1) for the different species are determined with the Lorentz−Berthelot mixing rule as

$$\sigma_{ij} = \left(\frac{\sigma_i + \sigma_j}{2}\right) \quad \text{and} \quad \epsilon_{ij} = \sqrt{\epsilon_i \epsilon_j} \tag{9}$$

with the parameters in the Table 1.

Methane adsorption is carried out in each structure at high pressure P = 200 MPa at T = 400 K, in order to fill the entire pore volume. The fluid loading (Γ_{CH_4}), is then adjusted by randomly removing molecules. All kerogen structures are finally relaxed by EMD simulations during 1 ns in the (N,P,T) ensemble, where the number of atoms N, the pressure P, and the temperature T are kept constant before averaging diffusion coefficients from the Green−Kubo (eq 2).

Methane adsorption was performed using a homemade grand canonical Monte Carlo algorithm. Molecular dynamic simulations were then performed using a Nosé−Hoover thermostat. The long-range bond order potential AIREBO[34,35] was used in order to model the covalent bonds of carbon atoms of the host, with a van der Waals cutoff set to 2 nm. The Green−Kubo integration was performed by a homemade Fortran code, interfaced with the open source Lammps package used as a library. It should be noted that the implementation of the AIREBO potential was subject to multiple bugs in Lammps versions anterior to March 2018. The autocorrelation velocity are built over a 40 fs, equilibrium averages were calculated at least 1000 times and the full averaging of the Green−Kubo equation was also performed 1000 times. Note that the simulations presented in this article are time-consuming. Each diffusion coefficient required at least 6 months of calculation running in parallel over 48 CPUs.

Table 1. Lennard-Jones Parameters for Carbon, Hydrogen, and Methane Molecules

atoms and pseudo atoms	σ (nm)	ϵ (meV)
CH_4	0.373	12.7
C	0.336	2.4
H	0.242	1.3

AUTHOR INFORMATION

Corresponding Author

Yann Magnin − *MultiScale Material Science for Energy and Environment, Massachusetts Institute of Technology-CNRS Joint Laboratory at Massachusetts Institute of Technology, Cambridge, Massachusetts 02139, United States;* orcid.org/0000-0002-4603-632X; Email: magnin@mit.edu

Authors

Jérémie Berthonneau − *Aix Marseille Univ, CNRS, CINaM, 13288 Marseille, France;* orcid.org/0000-0003-2354-5567

Nicolas Chanut − *MultiScale Material Science for Energy and Environment, Massachusetts Institute of Technology-CNRS Joint Laboratory at Massachusetts Institute of Technology, Cambridge, Massachusetts 02139, United States*

Daniel Ferry − *Aix Marseille Univ, CNRS, CINaM, 13288 Marseille, France*

Olivier Grauby − *Aix Marseille Univ, CNRS, CINaM, 13288 Marseille, France*

Rachel Jorand − *CVA Engineering, 64018 Pau, France*

Franz Joseph Ulm − *MultiScale Material Science for Energy and Environment, Massachusetts Institute of Technology-CNRS Joint Laboratory at Massachusetts Institute of Technology, Cambridge, Massachusetts 02139, United States*

Eric Chaput − *Total E&P Research & Development, 64018 Pau, France*

Roland Pellenq − *MultiScale Material Science for Energy and Environment, Massachusetts Institute of Technology-CNRS Joint Laboratory at Massachusetts Institute of Technology, Cambridge, Massachusetts 02139, United States;* orcid.org/0000-0001-5559-4190

Complete contact information is available at: https://pubs.acs.org/10.1021/acsanm.0c01191

Notes

The authors declare no competing financial interest.

ACKNOWLEDGMENTS

Y. Magnin, J. Berthonneau, N. Chanut, D. Ferry, O. Grauby, F. Ulm, and R. Pellenq aknowledge funding from TOTAL through the MIT/CNRS FASTER-Shale project. Y. Magnin also gratefully acknowledges TOTAL for the CPU time provided on their large super calculator PANGEA. Authors thanks J. Collell and D. Pantano (TOTAL) for fruitful discussions.

https://dx.doi.org/10.1021/acsanm.0c01191
ACS Appl. Nano Mater. 2020, 3, 7604−7610

REFERENCES

(1) Cueto-Felgueroso, L.; Juanes, R. Forecasting long-term gas production from shale. *Proc. Natl. Acad. Sci. U. S. A.* **2013**, *110*, 19660−19661.

(2) https://www.eia.gov/.

(3) Monteiro, P. J. M.; Rycroft, C. H.; Barenblatt, G. I. A mathematical model of fluid and gas flow in nanoporous media. *Proc. Natl. Acad. Sci. U. S. A.* **2012**, *109*, 20309−20313.

(4) Patzek, T. W.; Male, F.; Marder, M. Gas production in the Barnett Shale obeys a simple scaling theory. *Proc. Natl. Acad. Sci. U. S. A.* **2013**, *110*, 19731−19736.

(5) Vandenbroucke, M.; Largeau, C. Kerogen origin, evolution and structure. *Org. Geochem.* **2007**, *38*, 719−833.

(6) Clarkson, C. R.; Nobakht, M.; Kaviani, D.; Ertekin, T. Production analysis of tight-gas and shale-gas reservoirs using the dynamic-slippage concept. *SPE Journal* **2012**, *17*, 230−242.

(7) Rouquerol, J.; Avnir, D.; Fairbridge, C.; Everett, D.; Haynes, J.; Pernicone, N.; Ramsay, J.; Sing, K.; Unger, K. Recommendations for the characterization of porous solids (Technical Report). *Pure Appl. Chem.* **1994**, *66*, 1739−1758.

(8) Clarkson, C.; Solano, N.; Bustin, R.; Bustin, A.; Chalmers, G.; He, L.; Melnichenko, Y.; Radliński, A.; Blach, T. Pore structure characterization of North American shale gas reservoirs using USANS/SANS, gas adsorption, and mercury intrusion. *Fuel* **2013**, *103*, 606−616.

(9) Berthonneau, J.; Obliger, A.; Valdenaire, P.-L.; Grauby, O.; Ferry, D.; Chaudanson, D.; Levitz, P.; Kim, J. J.; Ulm, F.-J.; Pellenq, R. J.-M. Mesoscale structure, mechanics, and transport properties of source rocks' organic pore networks. *Proc. Natl. Acad. Sci. U. S. A.* **2018**, *115*, 12365−12370.

(10) Falk, K.; Coasne, B.; Pellenq, R.; Ulm, F.; Bocquet, L. Subcontinuum mass transport of condensed hydrocarbons in nanoporous media. *Nat. Commun.* **2015**, *6*, 6949.

(11) Bocquet, L.; Tabeling, P. Physics and technological aspects of nanofluidics. *Lab Chip* **2014**, *14*, 3143−3158.

(12) Won, C. Y.; Aluru, N. R. Water Permeation through a Subnanometer Boron Nitride Nanotube. *J. Am. Chem. Soc.* **2007**, *129*, 2748−2749.

(13) Obliger, A.; Pellenq, R.; Ulm, F.-J.; Coasne, B. Free Volume Theory of Hydrocarbon Mixture Transport in Nanoporous Materials. *J. Phys. Chem. Lett.* **2016**, *7*, 3712−3717.

(14) June, R. L.; Bell, A. T.; Theodorou, D. N. Molecular dynamics studies of butane and hexane in silicalite. *J. Phys. Chem.* **1992**, *96*, 1051−1060.

(15) Malek, K.; Coppens, M.-O. Knudsen self- and Fickian diffusion in rough nanoporous media. *J. Chem. Phys.* **2003**, *119*, 2801−2811.

(16) Sinha, S.; Braun, E.; Determan, M.; Passey, Q.; Leonardi, S.; Boros, J.; Wood, A., III; Zirkle, T.; Kudva, R. Steady-state permeability measurements on intact shale samples at reservoir conditions-effect of stress, temperature, pressure, and type of gas; SPE Middle East oil and gas show and conference, 2013.

(17) Falk, K.; Pellenq, R.; Ulm, F.; Benoit, C. Effect of Chain Length and Pore Accessibility on Alkane Adsorption in Kerogen. *Energy Fuels* **2015**, *29*, 7889−7896.

(18) Thran, A.; Kroll, G.; Faupel, F. Correlation between fractional free volume and diffusivity of gas molecules in glassy polymers. *J. Polym. Sci., Part B: Polym. Phys.* **1999**, *37*, 3344−3358.

(19) Obliger, A.; Ulm, F.-J.; Pellenq, R. Impact of Nanoporosity on Hydrocarbon Transport in Shales' Organic Matter. *Nano Lett.* **2018**, *18*, 832−837.

(20) Bhatia, S. K.; Bonilla, M. R.; Nicholson, D. Molecular transport in nanopores: a theoretical perspective. *Phys. Chem. Chem. Phys.* **2011**, *13*, 15350−15383.

(21) Frentrup, H.; Avendaño, C.; Horsch, M.; Salih, A.; Müller, E. Transport diffusivities of fluids in nanopores by non-equilibrium molecular dynamics simulation. *Mol. Simul.* **2012**, *38*, 540−553.

(22) Zwanzig, R. Time-Correlation Functions and Transport Coefficients in Statistical Mechanics. *Annu. Rev. Phys. Chem.* **1965**, *16*, 67−102.

(23) Cohen, M. H.; Turnbull, D. Molecular transport in liquids and glasses. *J. Chem. Phys.* **1959**, *31*, 1164−1169.

(24) Bhattacharya, S.; Gubbins, K. E. Fast Method for Computing Pore Size Distributions of Model Materials. *Langmuir* **2006**, *22*, 7726−7731.

(25) Bousige, C.; Ghimbeu, C.; Vix-Guterl, C.; Pomerantz, A.; Suleimenova, A.; Vaughan, G.; Garbarino, G.; Feygenson, M.; Wildgruber, C.; Ulm.; et al. Realistic molecular model of kerogen's nanostructure. *Nat. Mater.* **2016**, *15*, 576−582.

(26) Obliger, A.; Valdenaire, P.-L.; Capit, N.; Ulm, F. J.; Pellenq, R. J.-M.; Leyssale, J.-M. Poroelasticity of Methane-Loaded Mature and Immature Kerogen from Molecular Simulations. *Langmuir* **2018**, *34*, 13766−13780.

(27) Obliger, A.; Valdenaire, P.-L.; Ulm, F.-J.; Pellenq, R. J.-M.; Leyssale, J.-M. Methane Diffusion in a Flexible Kerogen Matrix. *J. Phys. Chem. B* **2019**, *123*, 5635−5640.

(28) Lin, D.; Liu, Y.; Liang, Z.; Lee, H.-W.; Sun, J.; Wang, H.; Yan, K.; Xie, J.; Cui, Y. Layered reduced graphene oxide with nanoscale interlayer gaps as a stable host for lithium metal anodes. *Nat. Nanotechnol.* **2016**, *11*, 626−632.

(29) Borchardt, L.; Leistenschneider, D.; Haase, J.; Dvoyashkin, M.s Revising the concept of pore hierarchy for ionic transport in carbon materials for supercapacitors. *Adv. Energy Mater.* **2018**, *8*, 1800892.

(30) Mitchell, S.; Pinar, A. B.; Kenvin, J.; Crivelli, P.; Kärger, J.; Pérez-Ramírez, J. Structural analysis of hierarchically organized zeolites. *Nat. Commun.* **2015**, *6*, 1−14.

(31) Chanut, N.; Wiersum, A. D.; Lee, U.-H.; Hwang, Y. K.; Ragon, F.; Chevreau, H.; Bourrelly, S.; Kuchta, B.; Chang, J.-S.; Serre, C.; et al. Observing the Effects of Shaping on Gas Adsorption in Metal-Organic Frameworks. *Eur. J. Inorg. Chem.* **2016**, *2016*, 4416−4423.

(32) Ning, Y.; He, S.; Liu, H.; Wang, H.; Qin, G.,et al..A rigorous upscaling procedure to predict macro-scale transport properties of natural gas in shales by coupling molecular dynamics with lattice Boltzmann method; SPE Annual Technical Conference and Exhibition, 2016.

(33) Adams, D. Grand canonical ensemble Monte Carlo for a Lennard-Jones fluid. *Mol. Phys.* **1975**, *29*, 307−311.

(34) Stuart, S. J.; Tutein, A. B.; Harrison, J. A. A reactive potential for hydrocarbons with intermolecular interactions. *J. Chem. Phys.* **2000**, *112*, 6472−6486.

(35) Magnin, Y.; Förster, G. D.; Rabilloud, F.; Calvo, F.; Zappelli, A.; Bichara, C. Thermal expansion of free-standing graphene: benchmarking semi-empirical potentials. *J. Phys.: Condens. Matter* **2014**, *26*, 185401.

https://dx.doi.org/10.1021/acsanm.0c01191
ACS Appl. Nano Mater. 2020, 3, 7604−7610